UFIFT-HEP-09-02
FERMILAB-PUB-09-044-T
April 10, 2009

Shedding Light on the Dark Sector with Direct WIMP Production

Partha Konar[1], **Kyoungchul Kong**[2], **Konstantin T. Matchev**[1], **Maxim Perelstein**[3]

[1] *Physics Department, University of Florida, Gainesville, FL 32611, USA*

[2] *Theoretical Physics Department, Fermilab, Batavia, IL 60510, USA*

[3] *Institute for High Energy Phenomenology, Newman Laboratory of Elementary Particle Physics, Cornell University, Ithaca, NY 14853, USA*

Abstract

A Weakly Interacting Massive Particle (WIMP) provides an attractive dark matter candidate, and should be within reach of the next generation of high-energy colliders. We consider the process of direct WIMP pair-production, accompanied by an initial-state radiation photon, in electron-positron collisions at the proposed International Linear Collider (ILC). We present a parametrization of the differential cross section for this process which conveniently separates the model-independent information provided by cosmology from the model-dependent inputs from particle physics. As an application, we consider two simple models, one supersymmetric, and another of the "universal extra dimensions" (UED) type. The discovery reach of the ILC and the expected precision of parameter measurements are studied in each model. In addition, for each of the two examples, we also investigate the ability of the ILC to distinguish between the two models through a shape-discrimination analysis of the photon energy spectrum. We show that with sufficient beam polarization the alternative model interpretation can be ruled out in a large part of the relevant parameter space.

1 Introduction

The most convincing and direct evidence for new physics beyond the Standard Model (BSM) is the existence of dark matter. The evidence for non-baryonic dark matter comes from a variety of observations on a wide range of astrophysical scales: rotation curves of galaxies, cosmic microwave background, gravitational lensing, mass to luminosity ratios from the motion of galaxies in clusters of galaxies, power spectrum and large scale structure, and so on. No particle in the Standard Model (SM) can account for the observed dark matter. Interestingly, many extensions of the SM at the electroweak scale possess good dark matter candidates. As the collider experiments begin directly probing this energy scale, it is important to understand what they can potentially teach us about dark matter.

If one assumes that the dark matter particle was in thermal equilibrium with the rest of the cosmic fluid in the early universe, and then decoupled once the temperature dropped, its present abundance can be predicted. In a generic case, the abundance is a function of two continuous parameters: the dark matter particle mass M_χ and its *total* annihilation cross section into SM states at low velocity, $\sigma_{\rm an}$. The current cosmological and astrophysical observations provide a measurement of the dark matter abundance, and indicate that the preferred values of $\sigma_{\rm an}$ are of order 1 pb. Interestingly, this also happens to be the typical cross section for processes mediated by the SM weak interactions or other weak-scale particles. This surprising coincidence provides an additional hint that the dark matter particle may indeed by a part of the weak-scale theory. The dark matter particles of this class are called Weakly-Interacting Massive Particles, or WIMPs.

There are two ways in which WIMPs can be produced in high-energy colliders. First, they can be directly pair-produced. (Since WIMPs are stable due to some new conserved quantum number, they cannot be singly produced in the collision of light SM particles.) Second, they can appear as decay products of other BSM particles. The second channel often has larger rates and smaller backgrounds, especially at the LHC where the production of strongly-interacting BSM states is enhanced. However, it is important to emphasize that this statement is very model-dependent and relies on the presence of *other*, heavier particles in the spectrum, which is a strong additional requirement independent of the WIMP dark matter hypothesis. In addition, the interpretation of the data in this channel is challenging. For example, the traditional methods for mass determination can provide a measurement of the WIMP mass only if long cascade decay chains are available and can be identified [1]. The measurement of the WIMP couplings to the SM states is also a very challenging task and even in best-case scenarios one can only determine certain combinations of couplings and mixing angles [2]. Moreover, the WIMP may be only one of several weakly-interacting new

particles present in the model, and it may be quite challenging to disentangle the features of this sector in cascade decays. For these reasons, direct production of WIMPs, while more challenging experimentally, may offer unique opportunities to study the WIMP in the lab.

The absence of a robust handle to distinguish events with direct WIMP production from the large SM background makes it virtually impossible to study this channel at the LHC [3, 4]. The relevant signatures (mono-jet plus missing energy and single photon plus missing energy) resemble direct graviton production in ADD models with Large Extra Dimensions [5], which is known to be among the experimentally most challenging searches at the LHC. Both channels are subject to a large irreducible background from Z + jets/photons, with Z decaying invisibly. In addition, there will be a large pure QCD background, where the missing energy arises as a detector effect. To make matters worse, the signal cross-sections in ADD are typically larger than the corresponding cross-sections for direct WIMP production. As a result of all these factors, the LHC is not expected to observe WIMPs directly, but only in the cascade decays of other, heavier particles. In this paper, therefore, we will consider the direct WIMP production at the proposed International Linear Collider (ILC), an e^+e^- collider with $\sqrt{s} = 500$ GeV. Most previous studies have analyzed this process in the framework of supersymmetry (SUSY), and correspondingly refer to it as "radiative neutralino production" [6, 7, 8, 9, 10, 11, 12, 13, 14, 15, 16, 17, 18, 19, 20, 21, 22, 23]. The related SUSY processes of direct production of sneutrinos or heavier neutralinos decaying invisibly, have also been considered [24, 25, 26, 27], leading to the so called "virtual LSP" scenarios. However, the connection between particle physics and cosmology provided by the WIMP hypothesis is very general, and is not restricted to supersymmetry. In particular, it may be readily applied in other model frameworks which have become popular in recent years, e.g. Universal Extra Dimensions (UED) [28, 29, 30, 31], Warped Extra Dimensions [32, 33, 34] and Little Higgs models with T-parity (LHT) [35, 36]. Given the multitude of existing models which can accommodate a successful WIMP, it is important to address the following two issues:

1. When predicting the size of any potential signals of direct WIMP production at colliders, how much of the discussion is model-independent, i.e. is relying only on the *generic* WIMP properties required by cosmology.

2. Once a signal of direct[1] WIMP production is observed, how can one discriminate among the various new physics model alternatives, e.g. SUSY, UED, LHT etc.

[1]Model discrimination from *indirect* WIMP production at the ILC was previously discussed in [37, 38, 39, 40].

The first question was addressed in Ref. [3], which developed the model-independent formalism for predicting the rate for direct WIMP production at colliders. Using detailed balancing, the production cross-section at colliders was related to the leading term $\sigma_{\rm an}$ in the velocity expansion of the WIMP annihilation cross-section (the procedure will be reviewed below in Section 2). It was shown that the collider signals can be uniquely predicted in terms of only two continuous parameters: the WIMP mass M_χ and the WIMP annihilation fraction κ_e into the e^+e^- final state (see the exact definition of κ_e in eq. (7) below). Interestingly, it turned out that the ILC has sensitivity to direct WIMP pair-production in an interesting parameter range for (M_χ, κ_e) [3, 41, 42, 43, 44], complementing more traditional methods for direct or indirect dark matter detection [43, 45].

While the formalism of Ref. [3] is attractive due to its model-independence, it has one significant drawback: in order to use the connection to cosmology, the WIMP's must be produced at low velocity, i.e. near threshold. On the other hand, the center-of-mass energy of the ILC may very well be far above threshold. In order to bring the WIMP system back near threshold, a hard cut on the energy E_γ of the associated photon was required [3], which lead to a significant reduction in the observable signal. In principle, the photon energy cut may be relaxed [43], which results in larger signal rates, but then the connection to cosmology is lost and the accuracy of the theoretical prediction goes awry.

In this paper, we tackle this problem by presenting a slightly modified framework to analyze this process. The new framework, outlined in Section 2, requires minimal additional inputs from the microscopic model of WIMPs, compared to the model-independent formalism of Ref. [3]. The advantage is that it allows to significantly relax the cut on the photon energy, extending the ILC reach. We also include the possibility of additional background suppression using polarized beams, further improving the reach [19, 20]. In Section 3 we show that once the observation is made, the ILC experiments can provide a measurement of the WIMP mass and the cross section of the process $e^+e^- \to \chi\chi$. The latter measurement is especially interesting, since if this cross section (at threshold) turns out to be larger than that indicated by the WIMP relic abundance, the χ particle will either be excluded as the sole dark matter component, or will require non-standard cosmology [46].

The second goal of this paper is to discuss the second question posed above: Once a signal of direct WIMP production is seen, how can one determine the WIMP properties and correspondingly the particular type of new physics model? This question has not been adequately addressed in the existing literature, since previous works on this channel have only considered one new physics model at a time, and did not attempt any model discrimination studies. In our case here, once our prediction of the observable photon spectrum becomes

model-dependent, a measurement of this spectrum can be readily used to distinguish between different models of WIMPs and their interactions. The results from such an analysis will be presented in Section 4.

2 Direct WIMP Production at the ILC

In this section, we will define the framework to describe a simple observable signature of the direct WIMP production in electron-positron collisions, and estimate the expected reach of the ILC in this framework.

2.1 The Signature

We consider the direct WIMP pair-production process

$$e^+e^- \to \chi\chi. \tag{1}$$

Here, the WIMP χ is an electrically neutral, color-singlet particle, with a mass in the 1 GeV-few hundred GeV range. At this point, we do not need to specify any other quantum numbers of χ (such as its spin), or the fundamental theory of which χ is a part. On its own, the process (1) does not leave an observable signature in the detector. To get an observable signature, we consider the closely related process

$$e^+e^- \to \chi\chi\gamma, \tag{2}$$

in which the WIMP pair can be observed as missing momentum recoiling against the detected photon. The cross section is dominated by the photons that are soft or collinear with the beam line:

$$E_\gamma \sin\theta \ll \sqrt{s}\,, \tag{3}$$

where E_γ is the photon energy, $\sqrt{s}$ is the center-of-mass energy of the collider and θ is the angle between the photon and the incoming electron. In this regime the differential cross section can be factorized according to the Weitszecker-Williams formula:

$$\frac{d\sigma_3}{dx\, d\cos\theta} = \mathcal{F}(x,\theta)\cdot\sigma_2(\hat{s})\,, \tag{4}$$

where $\sigma_3 \equiv \sigma(e^+e^- \to \chi\chi\gamma)$, $\sigma_2 \equiv \sigma(e^+e^- \to \chi\chi)$, $x = 2E_\gamma/\sqrt{s}$, $\hat{s} = s(1-x)$, and

$$\mathcal{F}(x,\theta) = \frac{\alpha}{\pi}\frac{1+(1-x)^2}{x}\frac{1}{\sin^2\theta}\,. \tag{5}$$

Of course, very soft or collinear photons remain undetected in a realistic detector; however, it was shown in Ref. [3] that the factorization (4) works rather well under realistic experimental conditions.

In general, the function $\sigma_2(s)$ depends on the microscopic model of the WIMP and its interactions with electrons. However, in the region close to production threshold, $s - 4M_\chi^2 \ll s$, this function can be approximated as

$$\sigma_2(s) \approx \sigma_0 \left(1 - \frac{4M_\chi^2}{s}\right)^{p+1/2} , \tag{6}$$

where p is the angular momentum of the lowest partial wave contributing to this process. (In particular, $p = 0$ for s-wave scattering and $p = 1$ for p-wave.) This is the approximation that was used in Ref. [3]. Its advantages are the independence from the underlying microscopic model, and the fact that the quantity σ_0 can be easily related to the relic abundance of the χ particle. The key relation is [3]

$$\sigma_0 = 2^{2(p-2)} \, (2S_\chi + 1)^2 \, \kappa_e \, \sigma_{\rm an} \, , \tag{7}$$

where S_χ is the spin of the χ particle, $\sigma_{\rm an}$ is the coefficient of the leading term in the small-velocity expansion of the total χ pair-annihilation cross section, and κ_e is the fraction of χ pair-annihilation events at low velocity which result in electron-positron pairs. At this point we also assume that $\chi = \bar{\chi}$, i.e. that the WIMP χ is identical to its antiparticle. This assumption will be true in our two examples discussed explicitly below, but is not really necessary in general – in the cases where $\chi \neq \bar{\chi}$, there is simply an additional factor of 2 in the right-hand side of (7).

The quantity $\sigma_{\rm an}$ is directly related to the present relic abundance of the χ particle. Assuming that χ makes up all of the observed dark matter, and using the observed value for the dark matter density $\Omega_{\rm dm} h^2 = 0.1143 \pm 0.0034$ [47], yields the determination of $\sigma_{\rm an}$ shown in Fig. 1. The quantity κ_e cannot be obtained from cosmology, and needs to be calculated once the model of particle physics is specified. Note however that in any model $\kappa_e \leq 1$, so that eq. (7) provides a model-independent upper bound on σ_0:

$$\sigma_0 \leq 2^{2(p-2)} \, (2S_\chi + 1)^2 \, \sigma_{\rm an} \, , \tag{8}$$

which is valid as long as χ is the dominant dark matter component. If the value of σ_0 measured in collider experiments turns out to violate the bound (8), there can be only two, equally exciting, explanations: that in addition to the χ particle, there must exist yet another independent WIMP candidate, or that there was some sort of non-standard cosmological evolution in the early universe.

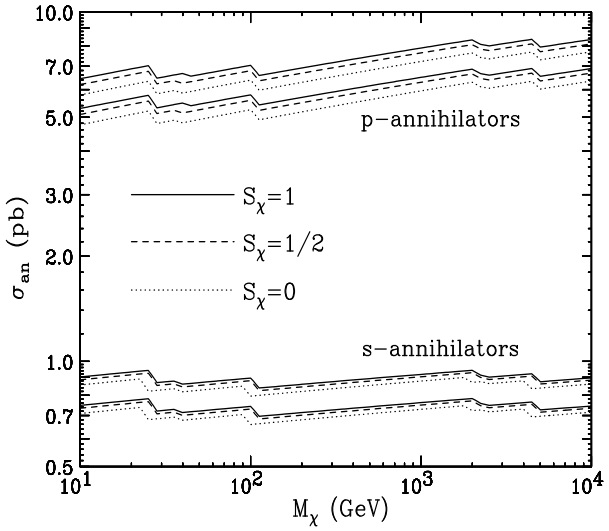

Figure 1: *Values of the quantity σ_{an} allowed at the 3σ level as a function of the WIMP mass M_χ, and for different values of the WIMP spin S_χ. The lower (upper) band is for models where s-wave (p-wave) annihilation dominates. We use the constraint $\Omega_{\rm dm}h^2 = 0.1143 \pm 0.0034$, which results from the combination of data from WMAP-5, Type Ia supernovae and baryon acoustic oscillations [47].*

The main disadvantage of the approximation (6) is its limited range of validity: if one wishes to use it to analyze data, one needs to impose a lower bound on the photon energy to restrict the analysis to the near-threshold region, thus cutting out most of the signal. In this paper, we will pursue a different approach: we will calculate $\sigma_2(s)$, for all values of s, in two benchmark models, and describe the ILC sensitivity for these models. As we will see, this gives a substantially better sensitivity than the model-independent search of [3]. To preserve the simple connection to relic abundance, we choose to parametrize the cross section as

$$\sigma_2(s) = \sigma_0\, f(s)\, \left(1 - \frac{4M_\chi^2}{s}\right)^{p+1/2} , \tag{9}$$

where $f(s)$ is a model-dependent dimensionless shape function obeying the normalization condition

$$f(4M_\chi^2) = 1\,. \tag{10}$$

This form reduces to eq. (6) in the near-threshold region, so the coefficient σ_0 is related to the relic abundance as described above.

Note that effects such as beamstrahlung [48] and the possibility of multiple ISR emission are not included in our approximation scheme. In the future, it would be interesting to incorporate these effects in the analysis.

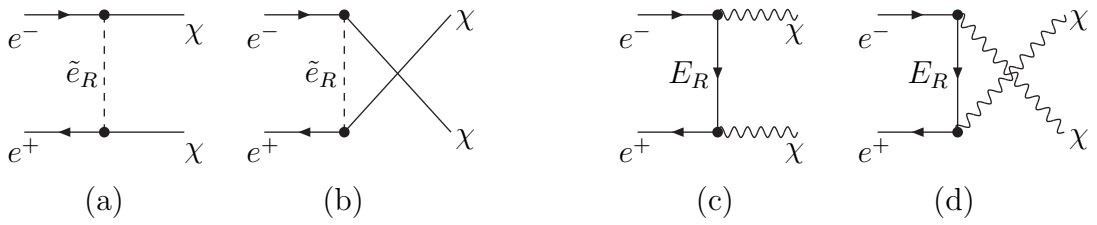

Figure 2: *Feynman diagrams for the WIMP pair-production in the SUSY benchmark model (a,b) and the UED benchmark model (c,d).*

2.2 Benchmark Models

Our first benchmark model is supersymmetric [49], with a pure Bino LSP pair-produced in electron-positron collisions via t-channel exchange of the right-handed selectron $\tilde{e}_R$, see the diagrams in Fig. 2 (a,b). This simple toy model approximates the constrained MSSM in the "bulk" dark matter region, up to subleading contributions due to non-bino admixtures in the neutralino and the heavier $\tilde{e}_L$ exchange. In this model, $p = 1$, since s-wave annihilation at threshold is forbidden by CP invariance (up to terms suppressed by $m_e^2/M_\chi^2 \sim 10^{-10}$, which we ignore). We obtain

$$\begin{aligned}
\sigma_0 &= \frac{g'^4}{12\pi M_{\tilde{e}_R}^2}\frac{z(1+z^2)}{(1+z)^4}\,, \\
f(y,z) &= \frac{3y^2(1+z)^4}{32z^2(1+z^2)(1-y)^{3/2}}\Big[\frac{4\sqrt{1-y}\,(y(1-z)^2+2z)}{y\,(y(1-z)^2+4z)} \\
&\quad + \left(-1+\frac{1}{z}+\frac{2z}{y(1-z)+2z}\right)\log\frac{y(1-z)+2z(1-\sqrt{1-y})}{y(1-z)+2z(1+\sqrt{1-y})}\Big]\,,
\end{aligned} \tag{11}$$

where

$$y \equiv \frac{4M_\chi^2}{s}, \quad z \equiv \frac{M_\chi^2}{M_{\tilde{e}_R}^2}\,. \tag{12}$$

Note that $0 < y, z \leq 1$, and that $\lim_{y\to 1} f(y,z) = 1$, as required by eq. (10). This is the cross section for unpolarized beams; since only right-handed electrons couple to $\tilde{e}_R$, the corresponding cross section for polarized beams can be found by simply multiplying by an overall factor of

$$(1+P_{e^-})\,(1+P_{e^+})\ , \tag{13}$$

where

$$P_{e^-} = \frac{n(e_R^-)-n(e_L^-)}{n(e_R^-)+n(e_L^-)}, \quad P_{e^+} = \frac{n(e_L^+)-n(e_R^+)}{n(e_L^+)+n(e_R^+)}. \tag{14}$$

are the electron and positron beam polarizations, respectively.

The second benchmark model is a spin-1 WIMP, pair-produced in electron-positron collisions via t-channel exchange of the spin-1/2 "heavy electron" E_R, see the diagrams in Fig. 2(c,d). The heavy electron is a Dirac fermion, and is assumed to be the partner of the right-handed electron e_R; this assumption fixes the helicity structure of the vertices in Fig. 2(c,d). This toy model reproduces the leading contribution to this process in the minimal UED model [29, 50, 51].[2] In this case, s annihilation is allowed, and $p = 0$. We obtain

$$\begin{aligned}
\sigma_0 &= \frac{g'^4 Y_{E_R}^4}{128\pi M_{E_R}^2}\frac{z}{(1+z)^2}, \\
f(y,z) &= \frac{y(1+z)^2}{128 z^5\sqrt{1-y}\Big(y(1-z)+2z\Big)\Big(y(1-z)^2+4z\Big)} \\
&\quad \Big[4z\sqrt{1-y}\Big(y(1-z)+2z\Big)\Big(y(1-z)^2(8z^2+3)+4z(8z^2-4z+3)\Big) \\
&\quad -\Big(y^2(1-z)^2(8z^2+3)+4yz(8z^2-6z+3)+8z^2(4z^2+1)\Big) \\
&\quad \Big(y(1-z)^2+4z\Big)\log\frac{y(1-z)+2z(1-\sqrt{1-y})}{y(1-z)+2z(1+\sqrt{1-y})}\Big],
\end{aligned} \tag{15}$$

where

$$y \equiv \frac{4M_\chi^2}{s}, \quad z \equiv \frac{M_\chi^2}{M_{E_R}^2}\,. \tag{16}$$

Note that we will continue to use the "generic" WIMP notation, χ, in the UED case; the χ in this case is actually the spin-1 massive partner of the hypercharge gauge boson, commonly known as B^1 [53].

Of course, it is straightforward to apply our formalism to other models, and we expect qualitatively similar results, as long as WIMPs do have an unsuppressed coupling to electrons. In all such cases the starting point of the analysis would still be the parametrization (9), from where the current discussion can be generalized in two different ways. First, one may consider a different region of parameter space of the same model (SUSY or UED), where there can be additional relevant diagrams beyond those shown in Fig. 2. For example, the addition of a t-channel $\tilde{e}_L$ exchange would simply modify the functional form of (11) and introduce an extra parameter (the mass of $\tilde{e}_L$). Alternatively, one may consider a different model altogether, by deriving the corresponding function $f(s)$ relevant for that case. From

[2]The unpolarized cross section is identical in the minimal Littlest Higgs model with T parity [52, 36], but the helicity of the vertices is the opposite, since only the left-handed electron has a partner in that model. Note also that the value of κ_e in the LHT model is small, of order 10^{-4}, due to a group theory factor suppression of the vertices in Fig. 2(c,d).

that point on, the analysis would still follow the steps outlined below for our two model examples (SUSY and UED).

2.3 ILC Reach

The above formalism provides a prediction for the differential rate of γ+missing energy events at an e^+e^- collider in terms of two continuous parameters, M_χ and σ_0, once a specific model is chosen to fix the function $f(s)$. Experiments at an e^+e^- collider can search for this signature as an excess over the SM background. We analyzed the reach of a 500 GeV ILC, assuming the following kinematic acceptance cuts:

$$\sin\theta \geq 0.1, \quad p_{T,\gamma} \equiv E_\gamma \sin\theta > 3 \text{ GeV}. \tag{17}$$

The $p_{T,\gamma}$ cut is imposed to reject backgrounds such as $e^+e^- \to e^+e^-\gamma$ in the region where the e^+ and e^- are too forward to be detected. This cut corresponds to the improved BeamCal acceptance of 6.67 mrad for 500 GeV linear collider [54]. With these cuts, the SM background is strongly dominated by the process $e^+e^- \to \nu\bar{\nu}\gamma$, and we ignore all other backgrounds in this study. We simulated this background using `CalcHEP` [55] and `CompHEP` [56]. To quantify the reach, we compare the differential cross sections $d\sigma/dE_\gamma$ for signal+BG and pure BG. To account for finite detector resolution, we smear the energy of the photon spectrum for both signal and background according to $\delta E/E = 14.4\%/\sqrt{E}_{\text{GeV}} \oplus 0.5\%$ [41]. We bin the events in 5 GeV bins in the photon energy, and compute the event numbers in each bin, $\{N^i_{\text{sig+BG}}\}$ and $\{N^i_{\text{BG}}\}$, for a given integrated luminosity $\mathcal{L}_{\text{int}}$. We then use the standard χ^2 technique to quantify the probability of measuring the event numbers predicted by the BG-only model if the true model is signal+BG. We define

$$\chi^2 = \sum_{i=1}^{N_{\text{bin}}} \frac{(N^i_{\text{sig+BG}} - N^i_{\text{BG}})^2}{N^i_{\text{BG}} + (\delta_{\text{sys}} N^i_{\text{BG}})^2}, \tag{18}$$

where δ_{sys} is the fractional systematic uncertainty in the background prediction. Note that we conservatively assume that this systematic error is uncorrelated between bins.

The reach of the search in the benchmark models defined above is presented in Fig. 3. We assumed an integrated luminosity of $\mathcal{L}_{\text{int}} = 500$ fb^{-1}, and a systematic error on the background prediction $\delta_{\text{sys}} = 0.3\%$. The 3σ evidence and 5σ discovery contours correspond to $\Delta\chi^2 = 9$ and 25, respectively. The contours labeled "polarized" correspond to electron and positron beam polarizations of $P_{e^-} = 0.8$ and $P_{e^+} = 0.6$, correspondingly. Note that these polarizations strongly suppress the dominant contribution to the background from t-channel W exchange, which only appears for left-handed electrons, while at the same time enhancing

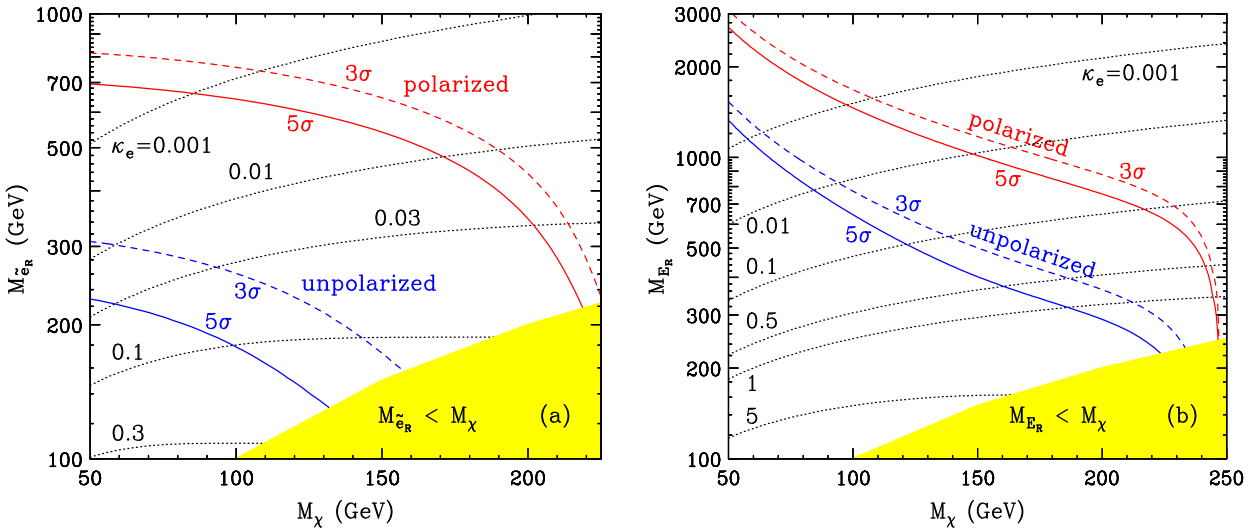

Figure 3: *The reach of a 500* GeV *electron-positron collider with an integrated luminosity of* $\mathcal{L}_{\rm int} = 500$ fb^{-1} *for discovery of our two benchmark models: (a) SUSY and (b) UED. Blue (red) lines correspond to unpolarized (polarized with* $P_{e^-} = 0.8$, $P_{e^+} = 0.6$*) beams. Solid (dashed) lines indicate* 5σ *(*3σ*) significance. Also shown are* κ_e *contours in the (a)* $(M_\chi, M_{\tilde{e}_R})$ *or (b)* (M_χ, M_{E_R}) *parameter plane.*

the signal in both of our benchmark models, where only the right-handed electrons couple to WIMPs. The reach is presented in terms of the WIMP mass and the mass of the t-channel particle which dominates the production process. One should keep in mind that the t-channel particle can also be directly produced at the ILC, provided its mass is within the kinematic reach of the collider. In this sense, one should note that the 5σ reach with unpolarized beams in the SUSY case of Fig. 3(a) only includes regions where the right-handed slepton $\tilde{e}_R$ would be directly produced as well. Consequently, in order to access the remaining parameter space where the radiative neutralino production is *the only* available signal, one must rely on beam polarization. In Fig. 3 we also show contours of constant κ_e, defined in eq. (7). For low WIMP masses, the reach of the ILC is impressive: with polarized beams, the WIMPs below 100 GeV can be discovered even if the e^+e^- channel only contributes 0.1% to the total WIMP pair-annihilation cross section in the early universe. For larger WIMP masses, the sensitivity decreases due to the kinematic suppression in WIMP production. This suppression can of course be compensated by a higher center-of-mass energy.

3 Parameter Measurement

Once the presence of non-SM contribution in the γ+missing energy channel is established, one can attempt to fit this contribution with BSM model predictions. In each model, the prediction depends on a number of unknown parameters; the fit to data can be used to constrain these parameters. In this section, we will discuss the accuracy of this procedure, using our benchmark models as examples. (Of course, it is possible that in a given model a good fit cannot be obtained for *any* sensible parameter values; in this case, the model would be ruled out as the interpretation of the data. We will discuss examples of such model discrimination in the next section.)

In the first example, we assumed that the data is given by the prediction of the SUSY benchmark model (plus SM background), with

$$M_\chi = 100 \text{ GeV}, \quad M_{\tilde{e}_R} = 300 \text{ GeV}. \tag{19}$$

For reference, these values correspond to $\kappa_e = 0.023$. We then performed a scan of the model parameter space, varying M_χ between 50 and 250 GeV, and $M_{\tilde{e}_R}$ between 100 and 1000 GeV. (We imposed $M_{\tilde{e}_R} > M_\chi$.) For each point in the scan, we computed the probability of observing the data given the model parameters at that point. To quantify this probability, we used the same χ^2 technique as in the reach analysis above. The results are presented in Fig. 4(a). With unpolarized beams, only a very crude mass determination is possible: for example, any WIMP mass up to 220 GeV is allowed at a 2-sigma level. With polarized beams, however, a rather impressive accuracy of about ± 20 GeV in both M_χ and $M_{\tilde{e}_R}$, at a 2-sigma level, can be achieved.

In Fig. 4(a) we also show contours of the quantity κ_e, which is uniquely fixed by eq. (7), once the values of M_χ and $M_{\tilde{e}_R}$ are specified. Therefore, a measurement of the parameters $(M_\chi, M_{\tilde{e}_R})$ can be immediately reinterpreted as a κ_e measurement. In particular, from Fig. 4(a) we see that with unpolarized beams, the ILC will only set an upper bound on κ_e of about 0.22 at the 3σ level, while using the polarized beam option, the κ_e determination is much more precise: $0.01 \leq \kappa_e \leq 0.04$ at 3σ.

In the second example, we repeated the same exercise for the UED benchmark model. The results, presented in Fig. 4(b), are qualitatively similar. The main difference in this case is quantitatively better sensitivity, mainly due to a higher signal cross section for the chosen model point ($M_\chi = 100$ GeV, $M_{E_R} = 300$ GeV, which in this case corresponds to $\kappa_e = 0.53$). As a result, a fairly accurate measurement of the masses is possible even with unpolarized beams: the accuracy on the WIMP mass is of order ± 10 GeV (± 20 GeV) at the 2-sigma (3-sigma) level. With polarized beams, a WIMP mass determination at the level of ± 2 GeV

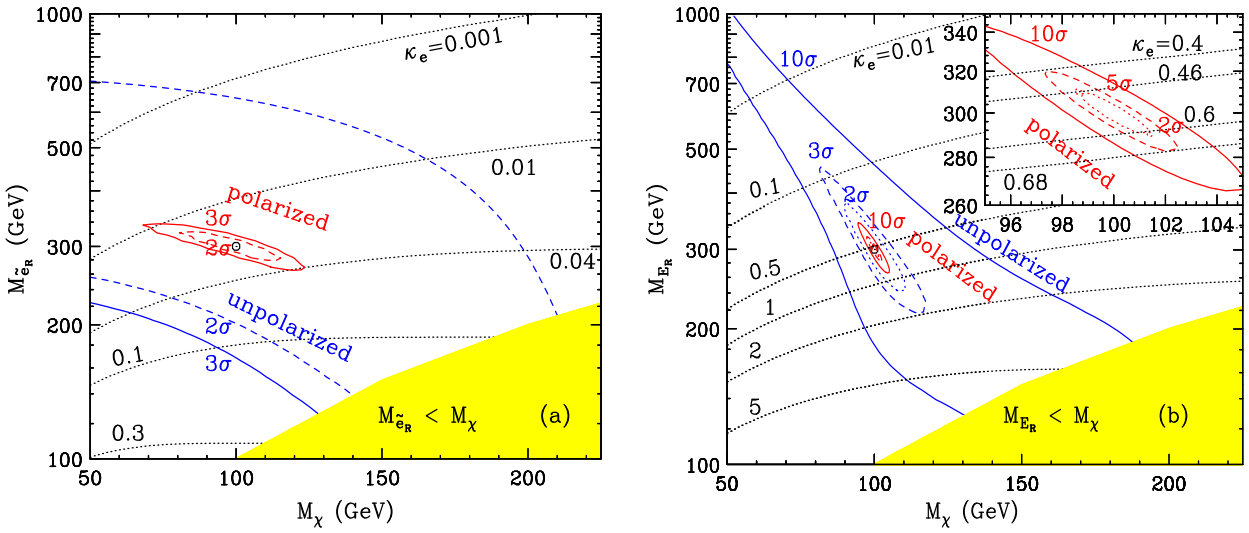

Figure 4: *Expected precision of the model parameter measurement in the two benchmark scenarios: (a) SUSY and (b) UED. The notation and labelling are the same as in Fig. 3.*

becomes possible. The corresponding 2-sigma determination of κ_e is now $0.2 \leq \kappa_e \leq 1.3$ ($0.46 \leq \kappa_e \leq 0.6$) with unpolarized (polarized) beams.

Note that the capability of the ILC to measure the WIMP mass in this process has also been recently analyzed by Bartels and List [44]. Their results for the spin-1 case (the only one analyzed in their study) are qualitatively in agreement with ours. Precise agreement is not expected, since the two studies used a different choice of the benchmark point, as well as a slightly different statistical analysis procedure - for example, Ref. [44] fits the WIMP mass M_χ assuming that κ_e is already known, whereas we perform a 2-parameter fit. Our results are also in qualitative agreement with those of Refs. [42, 43], which used the model-independent framework of [3] to perform a 2-parameter fit for (M_χ, κ_e).

4 Model Discrimination

Since the shape of the photon spectrum in the events with WIMP production is model-dependent (as characterized by the function $f(s)$), measuring this shape can provide interesting information about the underlying model. While not an unambiguous spin determination, this measurement can nevertheless distinguish scenarios in which WIMPs have different spins, as long as the WIMP interactions are specified in each model. As always, it is important to keep in mind that each of the models has free parameters, and a model can be "ruled out" only if the point in its *full* parameter space providing the *best fit* to data still does not provide an acceptable fit. (This point has been recently emphasized in Refs. [57, 2, 58].)

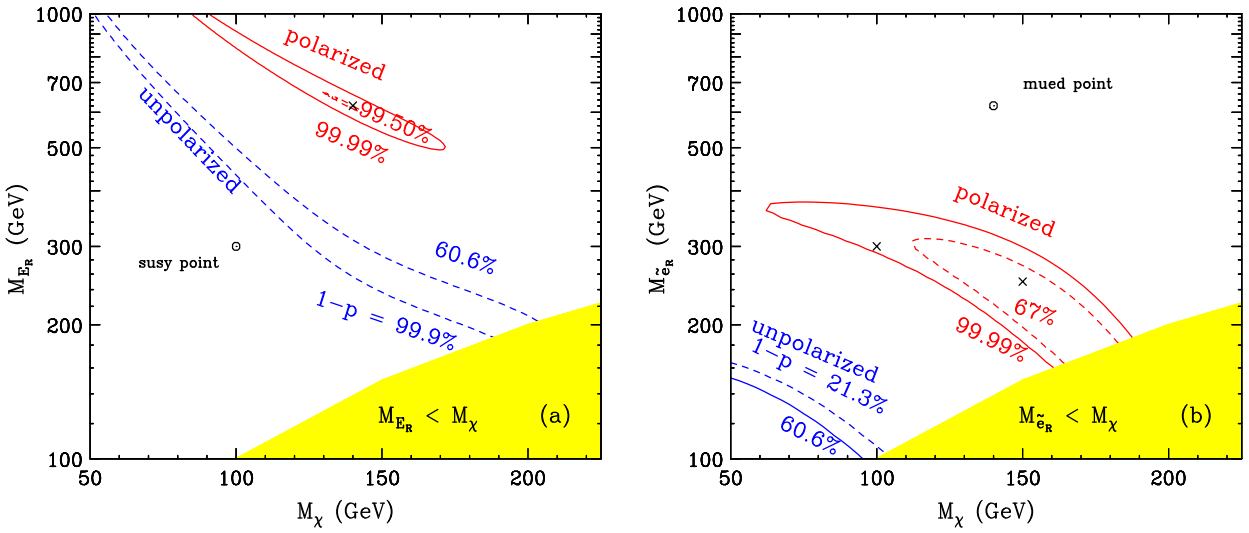

Figure 5: *Plots illustrating the ability of the ILC to discriminate between the two benchmark scenarios using the radiative WIMP production process.*

To illustrate the power of the ILC γ+missing energy measurements to distinguish between the two benchmark models, we performed two sample studies. In the first one, we assume that the data is given by the prediction of the SUSY benchmark model (plus SM background), with the same parameters as in eq. (19). We then attempt to fit the data with the predictions of the UED model, varying the parameters M_χ and M_{E_R}. For each parameter point, we determine the χ^2 value, and then compute the conditional probability p that the UED model with these parameters is true, given the data. The results are shown in Fig. 5(a). With unpolarized beams, the model-discriminating power of this measurement is rather poor: any UED model with parameters above the upper blue (dashed) contour could be true with probability above 40%. The UED model needs to be in the high-mass region to match the observed overall event rate, but since this rate is rather low and the background is high, there is not much sensitivity in this case. The model-discriminating power is greatly enhanced by beam polarization, which strongly suppresses the background and (in both of our benchmark models) enhances the signal. With polarized beams, the UED interpretation can be safely ruled out: even the best-fit point in the UED space (which happens to be at $M_\chi = 140$ GeV, $M_{E_R} = 621$ GeV) has only a 0.5% probability of describing the data. The photon spectra for the data (with polarized beams) and the best-fit UED point are shown in Fig. 6(a); it is clear from this figure that the quality of the UED fit to data is rather poor. One can conclude that the UED benchmark model as a whole is ruled out at a 99.5% CL by this data.

We repeated this analysis assuming that the true model is UED, with

$$M_\chi = 140 \text{ GeV}, \quad M_{E_R} = 621 \text{ GeV}, \tag{20}$$

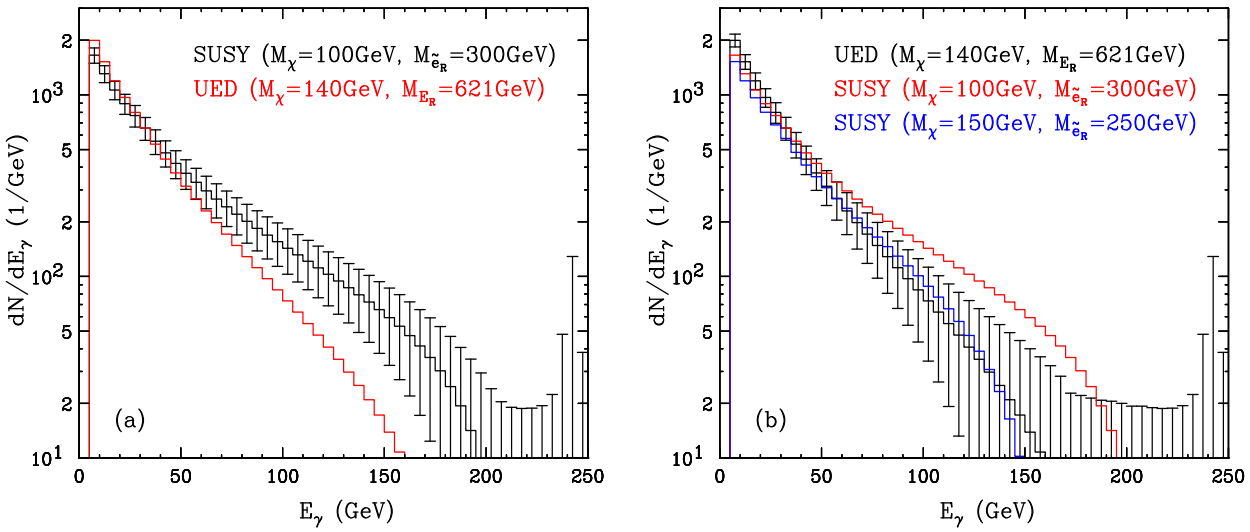

Figure 6: *Signal photon spectra in the two benchmark models. (a) Black histogram: SUSY model with the parameters in eq. (19); red histogram: UED model with parameters giving the best fit to the SUSY model. (b) Black histogram: UED model with the parameters in eq. (20); blue and red histograms: SUSY models with parameters as indicated by the two crosses in Fig. 5(a). In both cases, polarized electron and positron beams are assumed. The error bars on these "signal" histograms are derived from the full signal+BG distributions, with the statistical ($\mathcal{L}_{\rm int} = 500\ fb^{-1}$) and systematic (0.3%) errors, added in quadrature.*

and attempting to fit it with the SUSY predictions. The results are shown in Fig. 5(b). In this case, the model-discriminating power of the measurement is significantly weaker, primarily due to the low signal cross section. In the unpolarized case, most of the SUSY parameter space is allowed; only the points with low M_χ and $M_{\tilde{e}_R}$ are constrained. The situation is improved with the polarized beams, where most of the SUSY parameters space is ruled out at a confidence level of 99.9% or better. However, a significant part of the parameter space survives. This is clear from the photon spectra shown in Fig. 6: the "data" spectrum is well fit, within the error bars, by the predictions of sample SUSY points. The best-fit SUSY point, at $M_\chi = 170$ GeV, $M_{E_R} = 200$ GeV, gives a photon spectrum which is essentially identical to the input UED "data". Thus, convincing discrimination between the two models appears impossible in this case. However, this rather pessimistic conclusion is largely due to our choice of a relatively heavy UED study point. When we repeat the same analysis for the UED study point used in Fig. 4(b), namely $M_\chi = 100$ GeV and $M_{E_R} = 300$ GeV, we find that the SUSY interpretation is now completely ruled out.

The two models selected for our study differed in the behavior of the cross sections in the non-relativistic limit (s-wave for UED vs. p-wave for SUSY). This leads to a large difference

in the normalization factors σ_0 in the two models, see Eq. (8). However, by varying the masses, the overall rates of the two models can be made to agree, and it is the photon spectrum shape difference that is crucial for breaking that degeneracy. If instead we considered two models that both had, for example, s-wave annihilation, then the normalization σ_0 would be the same, and one would need to rely exclusively on the spectrum shape differences. As long as the spectra predicted by the two models are sufficiently different, model discrimination should be possible. Thus, the proposed technique should be useful in discriminating between models with the same threshold behavior of the WIMP annihilation cross section.

5 Conclusions

The ILC may offer a unique window into the dark matter world, by providing an opportunity to *directly* produce dark matter particles and study their properties. In this paper we revisited what is perhaps the most conservative and least model-dependent collider signature of dark matter: direct pair production of WIMPs, tagged with a photon from initial state radiation [3]. Our main results are as follows:

- We extended the formalism of Ref. [3] into the region away from the endpoint of the photon energy spectrum. The advantage of this new, although somewhat more model-dependent, approach is that it utilizes all of the available information from the single photon data, and not just near the endpoint. As a result, the discovery reach of the ILC is significantly improved, since one is going beyond a simple counting experiment, and using the measured shape of the spectrum as well.

- In Section 2.3 we estimated the ILC discovery reach for two representative models: SUSY and "UED"-like. In both cases we find that radiative WIMP production can be observable, as long as the WIMP mass is within the kinematic reach of the ILC and the WIMPs have non-negligible couplings to electrons. It is worth emphasizing the large difference in the reach with and without beam polarization – see Fig. 3.

- As demonstrated in Sec. 3, the ILC can determine the masses of both the WIMP and the associated t-channel particle (in our two examples, a slepton or a KK-lepton). This measurement is particularly impressive if beam polarization is available – see Fig. 4.

- Having observed a signal of radiative WIMP production, the ILC may also attempt a discrimination among different model explanations. The outcome of this analysis in general depends on the specific region of parameter space where the data happens to

lie, but as a rule, beam polarization significantly improves the chances for success – see Fig. 5.

Acknowledgments

We thank Hye-Sung Lee for collaboration in the early stage of this project. KM and MP would like to thank the Kavli Institute for Theoretical Physics (KITP) in Santa Barbara, where parts of this work were completed. PK and KM are supported in part by a US Department of Energy grant DE-FG02-97ER41029. MP is supported by the NSF grant PHY-0355005. Fermilab is operated by Fermi Research Alliance, LLC under Contract No. DE-AC02-07CH11359 with the U.S. Department of Energy.

References

[1] For a recent review comparing different mass measurement approaches, see M. Burns, K. Kong, K. T. Matchev and M. Park, JHEP **0903**, 143 (2009) [arXiv:0810.5576 [hep-ph]], and references therein.

[2] M. Burns, K. Kong, K. T. Matchev and M. Park, JHEP **0810**, 081 (2008) [arXiv:0808.2472 [hep-ph]].

[3] A. Birkedal, K. Matchev and M. Perelstein, Phys. Rev. D **70**, 077701 (2004) [arXiv:hep-ph/0403004].

[4] J. L. Feng, S. Su and F. Takayama, Phys. Rev. Lett. **96**, 151802 (2006) [arXiv:hep-ph/0503117].

[5] L. Vacavant and I. Hinchliffe, J. Phys. G **27**, 1839 (2001).

[6] P. Fayet, Phys. Lett. B **117**, 460 (1982).

[7] J. R. Ellis and J. S. Hagelin, Phys. Lett. B **122**, 303 (1983).

[8] K. Grassie and P. N. Pandita, Phys. Rev. D **30**, 22 (1984).

[9] T. Kobayashi and M. Kuroda, Phys. Lett. B **139**, 208 (1984).

[10] J. D. Ware and M. E. Machacek, Phys. Lett. B **142**, 300 (1984).

[11] L. Bento, J. C. Romao and A. Barroso, Phys. Rev. D **33**, 1488 (1986).

[12] M. Chen, C. Dionisi, M. Martinez and X. Tata, Phys. Rept. **159**, 201 (1988).

[13] T. Kon, Prog. Theor. Phys. **79**, 1006 (1988).

[14] C. H. Chen, M. Drees and J. F. Gunion, Phys. Rev. Lett. **76**, 2002 (1996) [arXiv:hep-ph/9512230]; arXiv:hep-ph/9902309.

[15] S. Ambrosanio, B. Mele, G. Montagna, O. Nicrosini and F. Piccinini, Nucl. Phys. B **478**, 46 (1996) [arXiv:hep-ph/9601292].

[16] S. Y. Choi, J. S. Shim, H. S. Song, J. Song and C. Yu, Phys. Rev. D **60**, 013007 (1999) [arXiv:hep-ph/9901368].

[17] H. Baer and A. Belyaev, in *Proc. of the APS/DPF/DPB Summer Study on the Future of Particle Physics (Snowmass 2001)* ed. N. Graf, *In the Proceedings of APS / DPF / DPB Summer Study on the Future of Particle Physics (Snowmass 2001), Snowmass, Colorado, 30 Jun - 21 Jul 2001, pp P336* [arXiv:hep-ph/0111017].

[18] H. K. Dreiner, O. Kittel and U. Langenfeld, Phys. Rev. D **74**, 115010 (2006) [arXiv:hep-ph/0610020].

[19] H. K. Dreiner, O. Kittel and U. Langenfeld, Eur. Phys. J. C **54**, 277 (2008) [arXiv:hep-ph/0703009].

[20] H. K. Dreiner, O. Kittel and U. Langenfeld, *In the Proceedings of 2007 International Linear Collider Workshop (LCWS07 and ILC07), Hamburg, Germany, 30 May - 3 Jun 2007, pp SUS05-POL01* [arXiv:0707.1642 [hep-ph]].

[21] R. Basu, P. N. Pandita and C. Sharma, Phys. Rev. D **77**, 115009 (2008) [arXiv:0711.2121 [hep-ph]].

[22] C. F. Berger, J. S. Gainer, J. L. Hewett, B. Lillie and T. G. Rizzo, arXiv:0712.2965 [hep-ph].

[23] S. K. Rai, Mod. Phys. Lett. A **23**, 73 (2008) [arXiv:0802.2209 [hep-ph]].

[24] F. Franke and H. Fraas, Phys. Rev. D **49**, 3126 (1994).

[25] A. Datta, A. Datta and S. Raychaudhuri, Phys. Lett. B **349**, 113 (1995) [arXiv:hep-ph/9411435].

[26] A. Datta, A. Datta and S. Raychaudhuri, Eur. Phys. J. C **1**, 375 (1998) [arXiv:hep-ph/9605432].

[27] A. Datta and A. Datta, Phys. Lett. B **578**, 165 (2004) [arXiv:hep-ph/0210218].

[28] T. Appelquist, H. C. Cheng and B. A. Dobrescu, Phys. Rev. D **64**, 035002 (2001) [arXiv:hep-ph/0012100].

[29] G. Servant and T. M. P. Tait, Nucl. Phys. B **650**, 391 (2003) [arXiv:hep-ph/0206071].

[30] H. C. Cheng, J. L. Feng and K. T. Matchev, Phys. Rev. Lett. **89**, 211301 (2002) [arXiv:hep-ph/0207125].

[31] B. A. Dobrescu, D. Hooper, K. Kong and R. Mahbubani, JCAP **0710**, 012 (2007) [arXiv:0706.3409 [hep-ph]].

[32] K. Agashe and G. Servant, Phys. Rev. Lett. **93**, 231805 (2004) [arXiv:hep-ph/0403143].

[33] K. Agashe, A. Falkowski, I. Low and G. Servant, JHEP **0804**, 027 (2008) [arXiv:0712.2455 [hep-ph]].

[34] G. Panico, E. Ponton, J. Santiago and M. Serone, Phys. Rev. D **77**, 115012 (2008) [arXiv:0801.1645 [hep-ph]].

[35] H. C. Cheng and I. Low, JHEP **0309**, 051 (2003) [arXiv:hep-ph/0308199].

[36] A. Birkedal, A. Noble, M. Perelstein and A. Spray, Phys. Rev. D **74**, 035002 (2006) [arXiv:hep-ph/0603077].

[37] M. Battaglia, A. Datta, A. De Roeck, K. Kong and K. T. Matchev, JHEP **0507**, 033 (2005) [arXiv:hep-ph/0502041].

[38] M. Battaglia, A. K. Datta, A. De Roeck, K. Kong and K. T. Matchev, *In the Proceedings of 2005 International Linear Collider Workshop (LCWS 2005), Stanford, California, 18-22 Mar 2005, pp 0302* [arXiv:hep-ph/0507284].

[39] B. Bhattacherjee and A. Kundu, Phys. Lett. B **627**, 137 (2005) [arXiv:hep-ph/0508170].

[40] M. R. Buckley, H. Murayama, W. Klemm and V. Rentala, Phys. Rev. D **78**, 014028 (2008) [arXiv:0711.0364 [hep-ph]].

[41] C. Bartels and J. List, *In the Proceedings of 2007 International Linear Collider Workshop (LCWS07 and ILC07), Hamburg, Germany, 30 May - 3 Jun 2007, pp COS02* [arXiv:0709.2629 [hep-ex]].

[42] P. Konar, "Something out of nothing: dark matter observation and mass determination in photon + missing energy events at the ILC", Talk given in the "Missing Energy" working group session, Joint Meeting of the American Linear Collider Physics Group ILC Global Design Effort, Fermilab, Batavia, Illinois, USA, 24 October 2007 (`http://ilc.fnal.gov/conf/alcpg07/`).

[43] N. Bernal, A. Goudelis, Y. Mambrini and C. Munoz, JCAP **0901**, 046 (2009) [arXiv:0804.1976 [hep-ph]].

[44] C. Bartels and J. List, arXiv:0901.4890 [hep-ex].

[45] A. Birkedal, K. T. Matchev, M. Perelstein and A. Spray, arXiv:hep-ph/0507194.

[46] D. J. H. Chung, L. L. Everett, K. Kong and K. T. Matchev, JHEP **0710**, 016 (2007) [arXiv:0706.2375 [hep-ph]].

[47] E. Komatsu *et al.* [WMAP Collaboration], arXiv:0803.0547 [astro-ph].

[48] A. K. Datta, K. Kong and K. T. Matchev, *In the Proceedings of 2005 International Linear Collider Workshop (LCWS 2005), Stanford, California, 18-22 Mar 2005, pp 0215* [arXiv:hep-ph/0508161].

[49] For a canonical review of supersymmetric dark matter, see G. Jungman, M. Kamionkowski and K. Griest, Phys. Rept. **267**, 195 (1996) [arXiv:hep-ph/9506380].

[50] K. Kong and K. T. Matchev, JHEP **0601**, 038 (2006) [arXiv:hep-ph/0509119].

[51] F. Burnell and G. D. Kribs, Phys. Rev. D **73**, 015001 (2006) [arXiv:hep-ph/0509118].

[52] J. Hubisz and P. Meade, Phys. Rev. D **71**, 035016 (2005) [arXiv:hep-ph/0411264];

[53] H. C. Cheng, K. T. Matchev and M. Schmaltz, Phys. Rev. D **66**, 036005 (2002) [arXiv:hep-ph/0204342].

[54] P. Bambade, V. Drugakov and W. Lohmann, Pramana **69**, 1123 (2007) [arXiv:physics/0610145].

[55] A. Pukhov, arXiv:hep-ph/0412191.

[56] A. Pukhov *et al.*, arXiv:hep-ph/9908288.

[57] C. Csaki, J. Heinonen and M. Perelstein, JHEP **0710**, 107 (2007) [arXiv:0707.0014 [hep-ph]].

[58] G. Hallenbeck, M. Perelstein, C. Spethmann, J. Thom and J. Vaughan, arXiv:0812.3135 [hep-ph].